Combined studies of gratings by X-ray reflectivity, GISAXS, and AFM

M. Yan,[a] J.F. Bardeau,[a] G. Brotons,[a] T. Metzger[b] and A. Gibaud [a*]

a- Laboratoire de Physique de l'Etat Condensé, UMR 6087 CNRS, Université du Maine, Faculté des Sciences, 72085 le Mans Cedex 09, France
b- European Synchrotron Radiation Facility (ESRF), BP 220, 38043 Grenoble Cedex, France

Abstract. The study of gratings has been carried out by different techniques such as specular and off-specular x-ray reflectivity, Grazing Incidence Small Angle X-ray Scattering (GISAXS) in coplanar and non coplanar geometries and atomic force microscopy (AFM). The comparison of the results is presented . The advantage of each technique is discussed. The new information obtained in GISAXS geometry concerning the very high sensitivity to the orientation of the gratings is commented.

INTRODUCTION

Surface gratings are beautiful synthetic objects exhibiting periodic arrays of grooves, lines and even dots. Their fabrication is nowadays perfectly mastered at the submicronic level but for technological applications, the trend is to go beyond this limit by targeting the nanometer scale. For instance, they remain of fundamental interest for applications in magnetic storage with the aim to achieve a density of dots allowing a storage capacity of one terabit or even more. Gratings have been also used in the past decade to study the coherence of x-ray beams at home laboratory and synchrotron facilities [1,2,3,4]. In this work, we have carried out the study of a series of gratings by means of X-ray techniques (such as X-ray reflectivity, Grazing Incidence Small Angle X-ray Scattering (GISAXS) in coplanar and non coplanar geometries) and atomic force microscopy (AFM). Our aim is to present the advantage of each technique in the analysis of these periodic objects.

The samples have been realized on the LETI Silicon platform (LETI-DPTS), within the framework of national RTB program. Starting from an SOI wafer (55nm Si / 145nm SiO_2 / Silicon bulk), features were defined by 193nm photolithography, followed by Silicon Reactive Ion etching. Using this process, gratings of different periods (400, 450 and 650nm)have been realized collectively, the height of the gratings being defined by the thickness of the SOI film.. Each motif was 1.5cm long and 1.4mm wide and altogether 9 motifs separated by a distance of 1.4mm were covering the surface of a given grating. The technology used for making the gratings is the Silicon On Insulator (SOI) technology for which a silicon layer of 55nm (nominal value) is deposited on a 145nm thick thermally grown silicon oxide. The silicon is then covered with a photosensitive resin that is insolated by UV light (λ=195nm) through the mask. The opaque zones of the mask prevent the exposition of the resin to UV radiation and correspond to the motifs that are replicated on the surface of the substrate. The typical periodic profile of a grating in which the relevant parameters describing the profile is shown in Fig. 1

METHODS OF INVESTIGATION

The easiest way to investigate the morphology of such gratings is to carry out direct imaging of the surface of these materials by Atomic Force Microscopy (AFM) or alternatively by Scanning Electron Microscopy (SEM).

* To whom correspondence should be addressed, gibaud@univ-lemans.fr

The AFM height images obtained by tapping mode are shown in Fig. 2. Periodic arrays of parallel stripes and dots are clearly seen on these images. With the mask designed by the LETI, the stripes were alternatively parallel to the x direction (Fig. 2a) or perpendicular to it (Fig. 2b). In addition an array of dots having a centered (Fig. 2c) and primitive (Fig. 2d) symmetry were also available. Quantitative information about the height of the lines or dots and the period of the gratings is readily obtained by AFM over a range going from of a few nm^2 to a few μm^2. Here we probe a height of 55 nm in full agreement with the expected nominal height of the silicon motifs. In addition the period of the motifs is also in perfect agreement with the nominal values. Of course, AFM does not provide any information about the silicon oxide layer on which the silicon motifs are located.

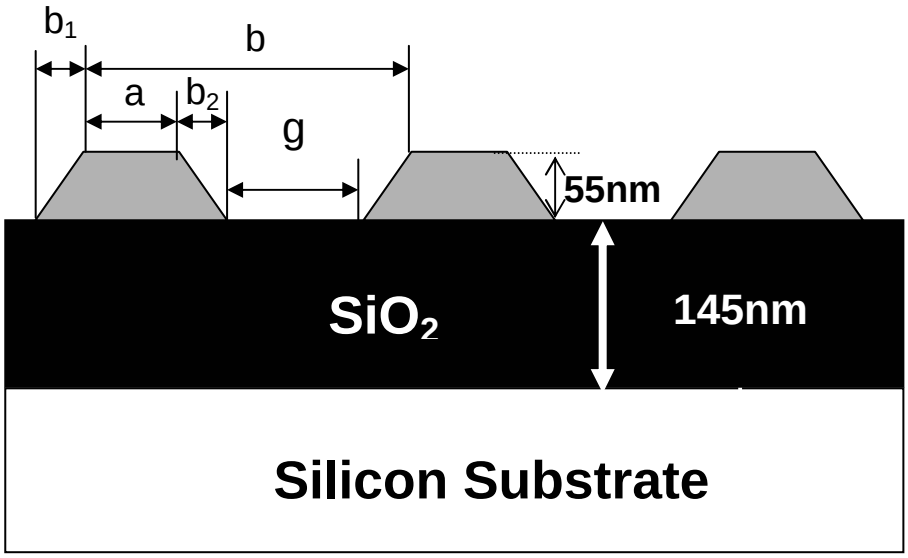

FIGURE 1. Sketch of a grating with the relevant parameters that are used to describe it.

The main drawback of the technique is indeed its lack of sensitivity to burried interfaces and the fact that images result in the convolution of the tip morphology with the real morphology of the relief. For large enough structures such as the ones investigated in this study this latter point is a minor problem but for motifs with dimensions of a few nanometers, this could become a serious problem.

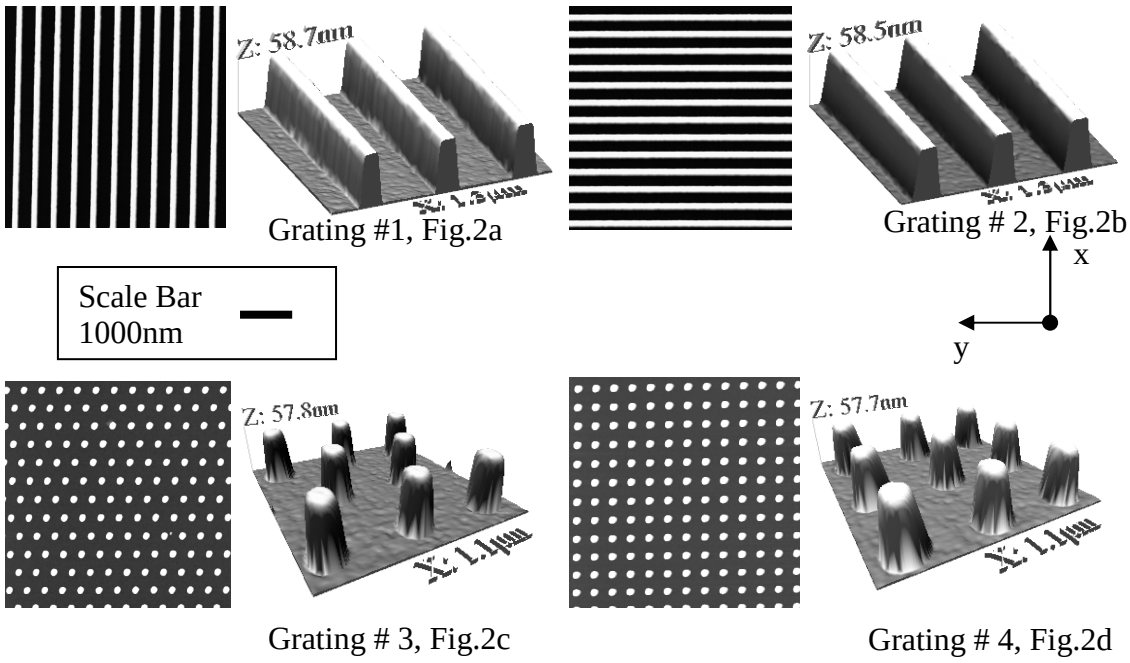

FIGURE 2. Typical AFM images of four different grating motifs. The scale bar is 1µm and is valid in both directions. Motif 1 exhibits a typical period of 450nm with lines of 150nm and grooves of 300nm along y (Fig 2a). Grating n°2 is similar but rotated by 90° about the normal to the surface of the substrate. Gratings 3 and 4 exhibits dots that were designed as square objects with a side of 200nm separated by 200nm. For all the motifs the height of the lines or dots was found to be 55nm in full agreement with the nominal value provided by the LETI.

On the opposite to AFM, x-ray scattering techniques do not provide a direct topography of the surface but information in reciprocal space. The information obtained in reciprocal space can be brought back in real space in means of a fitting procedure of the x-ray data. A model that describes the electron density profile of the grating (x,y and z directions) is used for calculating the x-ray reflectivity via the matrix formalism [5]. The calculated curve is compared to the measured one and the structural parameters are adjusted till a good agreement is found. This kind of investigation is definitely more demanding than what can be done with AFM direct space imaging. Fortunately scattering techniques provide essential information about the depth profile of electron density of the material. In addition any array presenting a periodic structure along a specific direction of reciprocal space will be easily detected by performing a scan of the wave vector transfer along this direction. Such scans provide statistical information integrated over a large area covered by the footprint of the incident beam on the surface of the material. The scattering pattern is therefore averaged on a large area (typically 1cm by 300µm) and is not a localized information like in AFM techniques.

Several geometries are available to address the scattering of a grating. Among them, one must distinguish between the coplanar and non coplanar geometries (see Figures 3 and 5). In coplanar geometry the direct and scattered beams are located in the plane of incidence (i.e. the plane containing the direct beam and the normal to the sample surface). In this geometry a series of scans can be carried out to map out the reciprocal space. Such scans are depicted in figure 3. The specular scan corresponds to the measurement of the X-ray specular reflectivity curve for which the incident and the scattering angles are equal and bisect the normal to the surface. The reflectivity scan gives the electron density profile in the direction normal to the surface. In the case of a grating the top surface of the grating has an average electron density lower than the substrate density due to the lack of material inside the grooves. The contrast of electron density gives rises to the usual Kiessig fringes related to the finite thickness of the film.

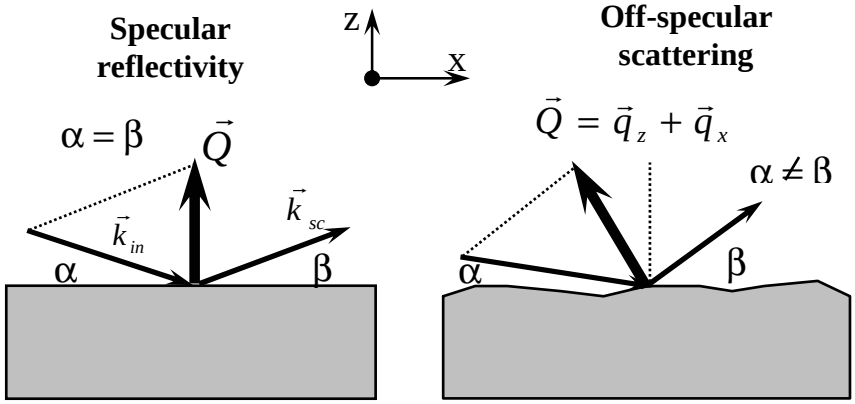

FIGURE 3. Illustration in coplanar geometry. of the wave vector transfers for specular and off-specular measurements. In all the following the x direction is the forward direction (direct beam direction at α=0).

An off-specular scan so-called rocking scan in Fig 3 allows one to probe the scattering features parallel to the surface of the sample in the x direction. For grating # 1, no periodic features are observed in the x direction and one does not expect any scattering along this direction except for the specular peak and the Yoneda wings due to the

surface roughness. This is quite different for the other gratings which exhibit a typical period along x. The scattering pattern contains different orders of diffraction as in classical optics grating diffraction experiments. A scan performed in this direction is limited by some inaccessible areas (see Fig 4) corresponding to either $\alpha=\alpha_c$ or $\beta=\alpha_c$ with α_c the critical angle of external reflection, namely the so-called Yoneda wings. The off-specular scan probes the scattering features in the plane of the substrate and is therefore similar to what can be obtained in GISAXS experiments in non coplanar geometry. Nevertheless in coplanar geometry the extension in q_x of a rocking scan is rather limited but the resolution function can be extremely narrow so that scattering features having a period of several µm can be seen. This is not the case in usual GISAXS experiments preformed in non coplanar geometry unless the detector is put at a very large distance from the sample (GIUSAXS) and we expect here a lower resolution for solving in-plane periodicities.

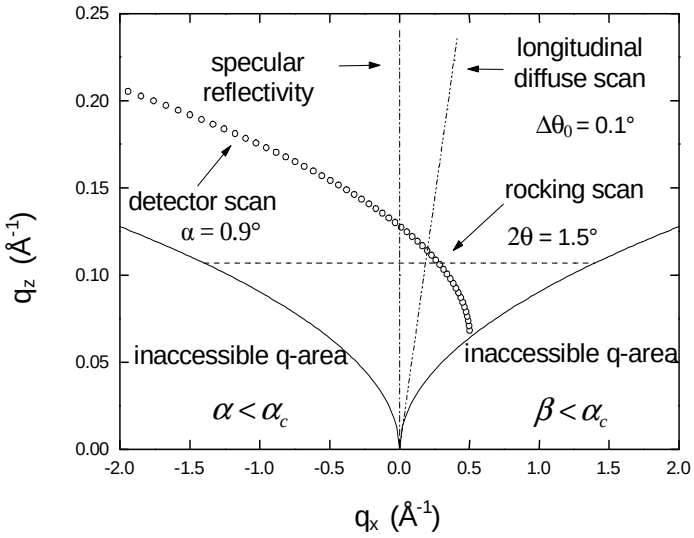

FIGURE 4 : Typical scans that can be performed in coplanar geometry. The inaccessible q areas correspond to the location of the Yoneda wings for which either the incident angle α or the exit angle β correspond to the critical angle of incidence (or below this angle). The rocking scan corresponds to a scan parallel to the surface in which the detector is kept at a fixed position while the incident angle varies. At small angles this scan is almost equivalent to a pure q_x scan with fixed q_z.

In non coplanar geometry, the incident and scattered beams are not in the same plane ($\varphi \neq 0$, see Fig 4). The angle of incidence is usually kept fixed to a value close to that of the critical angle and the scattered intensity is measured on a fixed 2D detector. The great advantage of the GISAXS measurement is that in non coplanar geometry, the accessible q_y range parallel to the surface is not limited by the sample surface like it is in coplanar geometry. On the other hand the resolution is generally not as good as in coplanar geometry so that the two techniques are complementary. In the case of gratings the other advantage is that the coplanar and non coplanar geometries allows one to measure the periodicity in the two perpendicular direction of the sample surface. The non coplanar geometry is ideal to probe a periodicity along the q_y direction. Note that both directions (x and y) are not equivalent for such gratings.

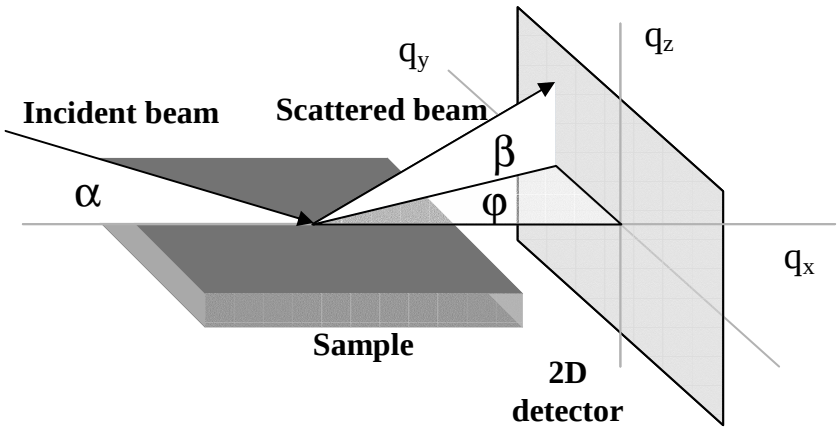

FIGURE 5. Illustration of the GISAXS geometry (non coplanar geometry). The angle of incidence, α, is fixed and the scattered beam is collected on a 2D detector.

RESULTS OF THE SCATTERING EXPERIMENTS

Results obtained in coplanar geometry

Figure 6 shows the X-ray reflectivity curves of grating number 2, i.e. the grating for which the lines are perpendicular to the incident beam. We wish to point out here that the total reflection plateau area is quite difficult to measure and to analyze in the case of such a grating. This is why we only analysed the data in the range q_z=0.15 to 0.36A^{-1}. As expected the pattern exhibits Kiessig fringes which present a beating due to a difference of electron density between the substrate itself, the thermally grown SiO_2 covering the silicon substrate and the silicon lines of the grating. The Fourier analysis of the beating immediately yields two specific thickness t_1=55nm and t_2=142.6nm as shown in the inset of Fig. 6. These values were used to carry out the calculation of the reflectivity pattern via the matrix formalism [5]. The height of the silicon lines that are located above the SiO_2 is fully confirmed by AFM (see Fig.2) and by our analysis of the X-ray reflectivity pattern. The calculation of the X-ray reflectivity pattern yields an electron density of the top layer of 240e^-/nm^3 whereas the electron density of the SiO_2 was fixed to 790 e^-/nm^3. The value of the electron density of the top layer made of silicon lines with a density of 720 e^-/nm^3 separated by emptied grooves is in good agreement with a surface coverage of 1/3 for this grating. Note that the density of the thermally grown oxide was constrained because the measurements were not made in absolute scale and that the critical angle region is useless in this case. Similar scans were obtained for the other gratings shown in Figure 2.

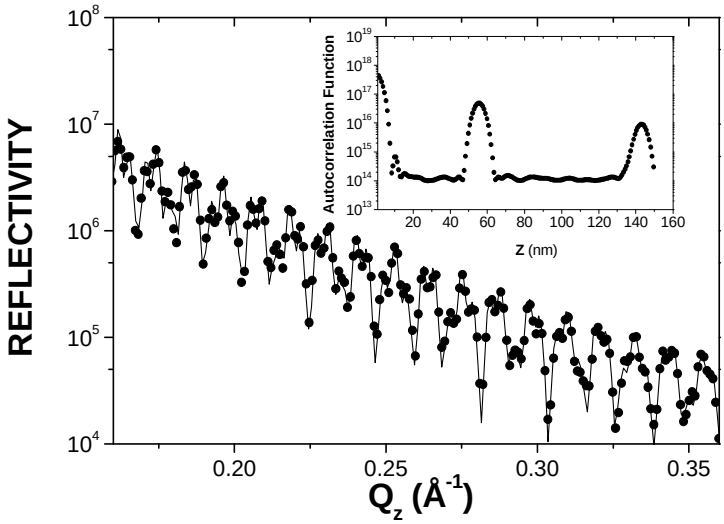

FIGURE 6. Calculated and observed X-ray reflectivity curves of grating number 2. The autocorrelation function of the derivative of the electron density is shown in the inset. Two peaks are clearly seen around 55nm and 142nm. These values were used as input for the calculation of the X-ray reflectivity by the matrix technique.

The periodic structure of a grating produces a diffracted pattern showing equally spaced peaks when the scan is performed parallel to the periodic direction of the grating. Fig. 7 shows a typical q_x scan (rocking scan) measured at a scattering angle of 3° on grating number 2 of Fig. 2. The characteristic orders of diffraction are well observed. Their location, limited by the position of the Yoneda wings, provides a very sensitive information about the period, *b*, of the grating since each order, *n*, is located at $q_x = 2\pi n / b$.

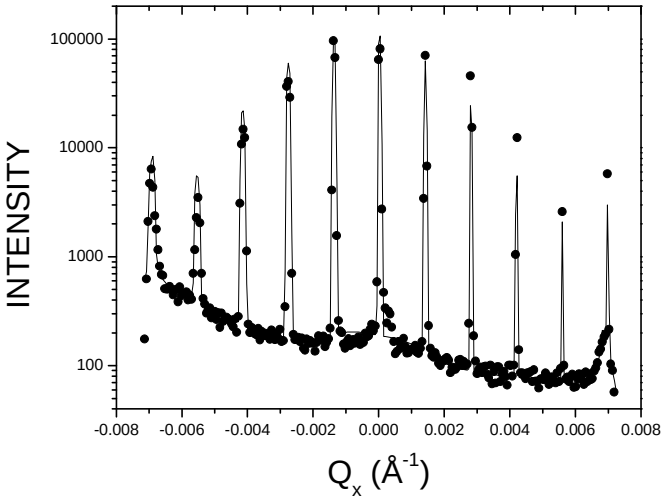

FIGURE 7. Calculated and observed transverse scans for grating number 2. The scans exhibit peaks corresponding to scattering orders of the grating. The extension of the observed peaks is limited in this kind of scans by the Yoneda peaks.

The pattern in figure 7 is calculated according to the formalism developed by M. Tolan et al.[6]. The period of the grating is found to be *b*=451.6nm in full agreement with the nominal value of 450nm. Although the fit is quite correct, we have found that the sensitivity to parameters such as the width, *g*, of the grooves or the trapezoidal shape (parameters b_1, b_2 and *a* in Fig. 1) is somehow small. This might be related to the fact that the number of measured orders is limited to 5 with one of them located beyond the Yoneda edge. A scan performed at a higher scattering angle of next orders would help to constrain these parameters. The fit yields to a groove that is 309nm wide and an asymmetric shape for the lines with parameters a=61nm, b_1=52nm and b_2=28nm. The asymmetry of the shape is dubious in view of the AFM images that look quite symmetric thus it highlight the low sensitivity of the x-ray rocking scan analysis to such asymmetry. The parameters are nevertheless in agreement with the fact that the grating does not exhibit a square profile since otherwise the intensity of the third order would have been extinct. Let us also point out that the width of the different orders decreases when the q_x wave vector transfer goes from negative to positive. This is in full agreement with our previous study of such effect [7].

Similar results were obtained for the three other gratings (see Figure 8). Grating number 1 does not exhibit any diffraction orders in the rocking scans since the incident beam is parallel to the lines of the grating. Gratings 3 and 4 give very nice and symmetric patterns that are in full agreement with the AFM images. In particular the spacing between the orders is doubled for grating 3 compared to grating 4. This is fully expected since the period of these two gratings are 800 and 400nm.

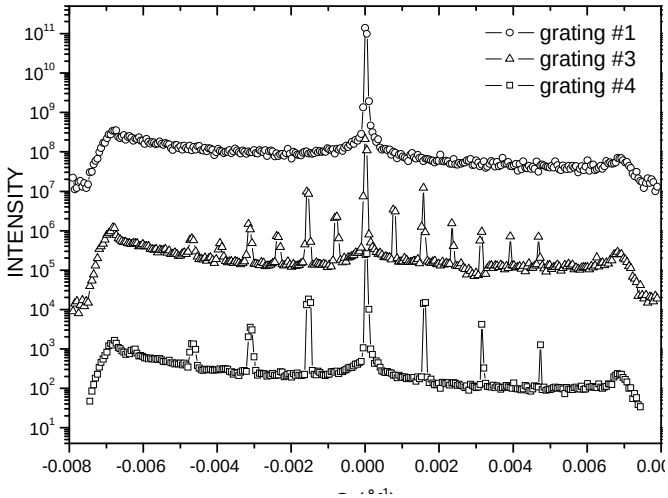

FIGURE 8. Observed transverse scans for gratings number 1, 3 and 4. Grating 1 does not exhibit any period along qx. The period of grating 4 along this direction is half of the one of grating 3.

GISAXS results obtained in non coplanar geometry

Very systematic measurements were obtained in the GISAXS experiments. In particular we found that the GISAXS patterns measured when the grating lines are almost parallel to the direct beam, are very sensitive to any change in the azimuthal angle. The grating can be easily aligned to better than 0.01° just by looking at the changes of the GISAXS patterns as shown in Figure 9 for the three orientations ψ=0°,-1° and 1°. This effect was already pointed out by Mikulik et al. [8,9] in their study of W/Si multilayer gratings.

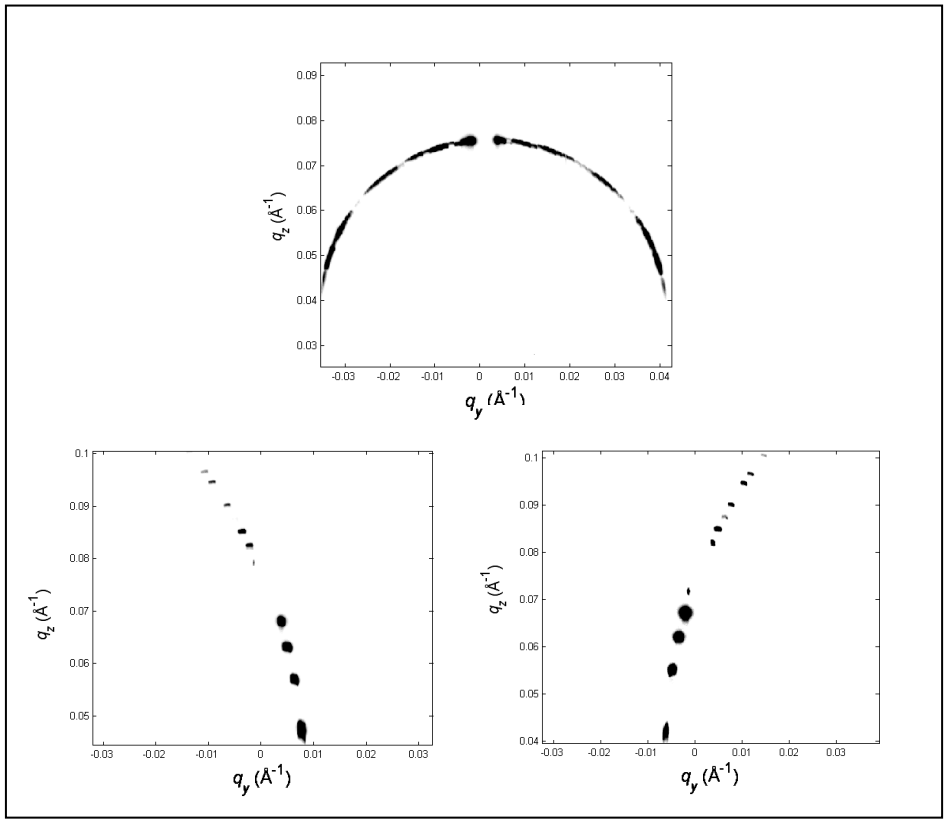

FIGURE 9. GISAXS pattern of .grating #1 for three different azimuthal rotation ψ=0°,-1° and 1°. The top image(ψ=0°) shows a a series of fringes located on a hemi-circle. The bottom images (ψ=1° left and -1° right) exhibit fringes corresponding to the intersection of the grating truncature rods (GTR) with the Ewald sphere.

The pattern observed at ψ=0° is not located on a straight line but on a circle of radius $q_r = \sqrt{q_z^2 + q_y^2}$ equal to about half of the wave vector transfer q_z=0.08 Å^{-1}at q_y=0. Note that this value corresponds to the wave vector transfer of the specularly reflected beam corrected from the refraction effect. It is directly defined by the incident angle of the direct beam with the surface of the grating. The circular shape of the scattering can be explained by considering the intersection of the Ewald Sphere with the q_x=0 plane that is rotated by an angle of 0.4° with respect to the direct beam. This plane contains the grating truncation rods (GTR) that run perpendicular to the surface of the grating every $q_y = 2\pi n / b$ [10]. The GTR are located in the plane q_x=0 and have a long extension in q_z (since the height of the motif is small) and are periodically spaced along q_y (because of the period in y). The intersection of the Ewald sphere with these rods gives a circle with peaks that are only visible above the horizon of the sample as shown in Figure 10.

As soon as the grating is rotated about the azimuthal axis (see bottom panels of Figure 9) the projection of the circle on the 2D detector becomes completely distorted. A series of spots reminiscent of the ones seen on the circle and due to the GTR appear along a curved line. These spots are very well separated due to the distortion.

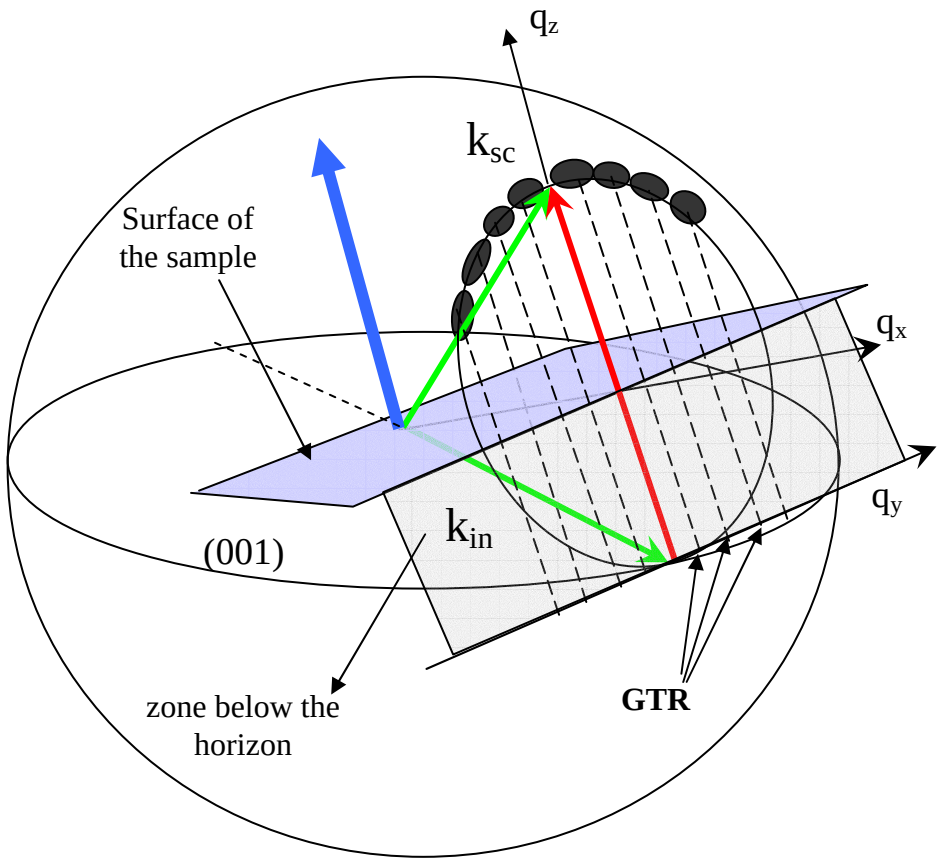

FIGURE 10. Illustration of the intersection of the plane q_x=0 at ψ=0 with the Ewald sphere. The GTR (dotted lines) located along q_y are equally spaced every $q_y = 2\pi n / b$. The horizon of the sample precludes the observation of a complete circle so that the intersection of GTR with the Ewlad sphere is located on a hemi-circle.

The pattern at ψ=0° exhibits fringes that are modulated in intensity. The period of the fringes is consistent with the period of the grating and so is the modulation with the form factor of the lines. For instance the motif shown in

figure 6 has a period of 450nm with lines that are nominally 150nm wide. Therefore, one expects to have fringes located every $2\pi/4500=0.0015$ Å^{-1} with a period of modulation every 0.0045Å^{-1}. This is close to what is shown in Fig 11.

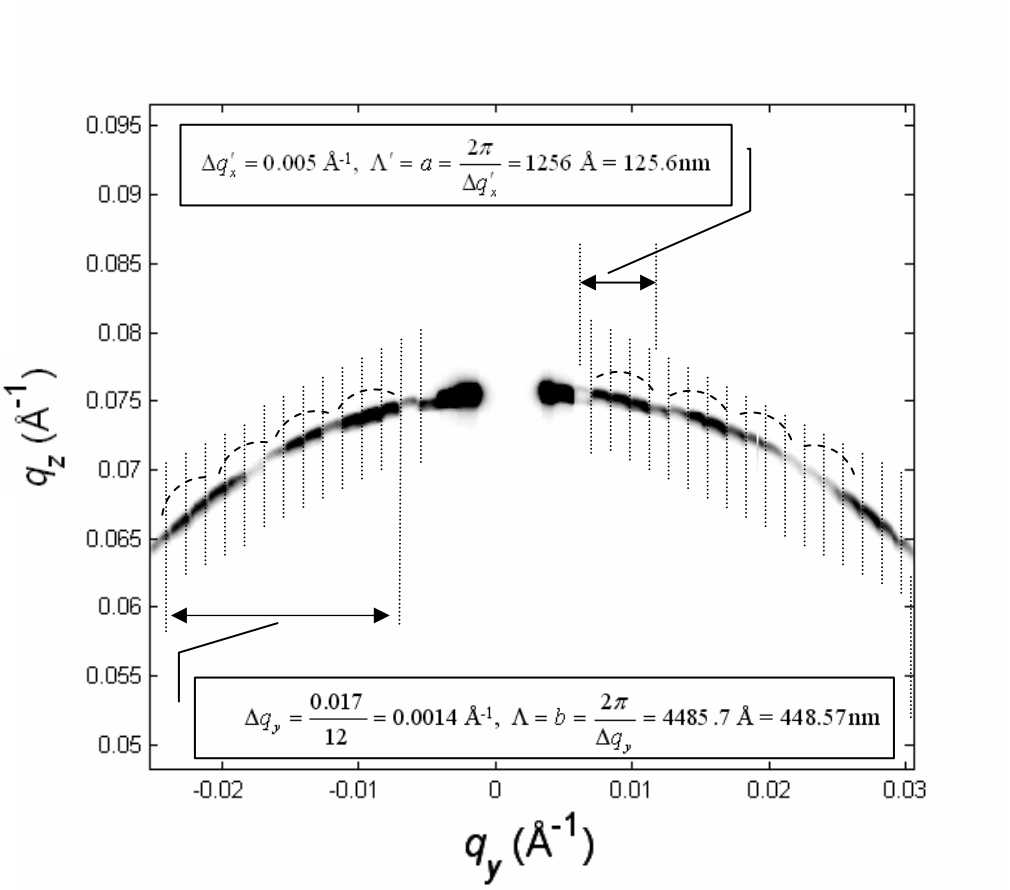

The series of spots seen on figure 9 when the grating is rotated about its normal are also well interpreted in terms periodicity. A more detailed analysis of the location of these spots will be soon reported.

CONCLUSION

We have shown in this paper that x-ray scattering techniques used in coplanar and non-coplanar geometries are very well suited to study the morphology of gratings. The results are in very good agreement with the AFM images of the morphology. In addition the reflectivity allows the probe the presence of buried interfaces. In GISAXS the grating truncation rods give rise to stunning effects when intersecting the Ewald sphere at different azimuthal angles. This allows to orient the grating with a tremendous accuracy.

ACKNOWLEDGMENTS

The authors are greatly indebted to the ESRF for the use of the ID01 beam line and to the CEA, LETI, Minatec® innovation center for providing the gratings. Special thanks are addressed to Denis Renaud for his kind help to design the gratings and to P. Lyan, A De Luca from the LETI.

REFERENCES

1. Tolan M., Ph. D. thesis University of Kiel (1993).
2. Tolan M.,Kong G.,Brugemann L.,Press W.,Brinkop F. and Kotthaux J.P., Europhys.Lett. 20 pp.223 (1992)
3 Tolan M.,Bahr D.,Sussenbach J.,Press W.,Brinkop F. and Kotthaus J.P. Physica B 198 pp.55 (1994)
4. Tolan M.,Rhan H.,Metzger T.H.,Peisl J.,Schuster R.and Kotthauss J.P., Z. Phys. B 96 pp.227 (1994)
5. X-Ray and Neutron Reflectivity: Principles and Applications, Eds. Jean Daillant and Alain Gibaud, Spinger 1999 (ISBN 3-540-66195-6).
6. Tolan M., Press W., Brinkop F. and Kotthaus J.P., J.Appl.Phys., 75, pp.7761 (1994).
7. Gibaud A.,Wang J., Tolan M.,Vignaud G. and Sinha S.K., J.Phys. I France 6 pp. 1085-1094 (1996)
8. Mukulik P.,Jergel M.,Baumbach T.,Majkova E.,Pincik E.,Luby S.,Ortega L.,Tucoulou R.,Hudek P. and Kostic I., J.Phys.D:Appl.Phys.34 pp.A188-A192 (2001)
9. Mikulik P.,Baumbauch T., Physica B pp.381-386 (1998)
10. Jergel M.,Mikulik P.,Majkova E.,Luby S.,Senderak R.,Pincik E.,Brunel M.,Hudek P.,Kostic I. and Konecnikova A. J.Phys.D:Appl.Phys.32 pp.A220-A223 (1999)